ISSN 1330-3651 (Print), ISSN 1848-6339 (Online)
https://doi.org/10.17559/TV-20210715110322
Original scientific paper

Effect of Slow Solidification of Ultra-thick Continuous Casting Slab on Solidification Structure and Macrosegregation

Jiazheng ZHANG, Ling YAN, Changjun XU*, Dejun LI*, Lianwang ZHANG

Abstract: The slow solidification method of ultra-thick slab is in the ascendancy, and the macrosegregation is an important parameter of slab quality. Besides, solidification structure is also a crucial indicator of slab, such asSecondary Dendrite Arm Spacing (SDAS). In this paper, the slice moving boundary model was selected and optimized, and the influence on SDAS and macro segregation under slow solidification condition are investigated. Researches show that the SDAS increases by increasing supercooling and cooling intensity. When the superheating increases from 20 K to 40 K, the SDAS increases from 156,8 μm to 158,9 μm. By using mid-strong cooling, the segregation ratio decreases from 1,4331 to 1,3836, and the segregation degree decreases from 0,3535 to 0,3196. According to the discussions, a new method of improving the final quality of slow solidification continuous casting slabs is provided, which also has a high development prospect in the production of large-section casting slabs.

Keywords: macro segregation; SDAS; solidification structure; superheating; ultra-thick slab

1 INTRODUCTION

Ultra-thick slab is a high value-added product; it is frequently used in military industry, nuke industry, marine engineering and engineering machinery. The common pattern of ultra-thick slab production is continuous casting; it has high efficiency and low energy cost [1-3]. With the development of slab continuous caster, the thickness of slab is also increasing. The ultra-thick slabs with 450 mm thickness were manufactured in Xingcheng Special Steel Co., Ltd in 2008. Ansteel Co., Ltd in China had also produced 300 mm thickness slabs in 2009. Dillingen in Germany produced a 600 milimiter thickness ultra-thick slab in 2017 [4], and took the producible thickness of ultra-thick slab to a new level.

The amount of molten steel in ultra-thick slab is large. In order to prevent bleed-out, a low casting speed should be used during solidification process. The low casting speed extends the solidification time and reduces the cooling rate. The solidification rate is usually lower than 10^{-3} ~1 K/s [5], which can be regarded as slow solidification. The slow solidification method of ultra-thick slab is in the ascendancy. With the increasing thickness of ultra-thick slab, more attention will be paid to this new technology. However, the internal quality issue of the slab, such as macro segregation, should be improved.

Simulations and experiments have been taken to investigate the mechanism of segregation. Xiao et al. believed that the segregation is the effect of movement of segregated residual liquid with respect to the mushy zone [6]. The type of segregation can be eliminated by changing cooling intensity of secondary cooling zone [7]. An et al. [8] and Wisileietal [9] suggested that the segregation between dendrites is mainly influenced by dendrite arm spacing (DAS). Long et al. concluded that large spacing of dendrite will cause internal defect or production accident of slab [10]. Previous studies on thin slabs and square billets also show that the length of primary dendrite arm spacing is related to temperature gradient and dendrite growth rate; and the secondary dendrite arm spacing (SDAS) is only related to cooling rate for the same material. According to the research above, unreasonable cooling intensity and large SDAS cause macro segregation. However, few studies had been conducted under slow solidification of ultra-thick slab.

In current industrial production, most of the large-section casting slabs are produced by slow solidification method. In this paper, the ultra-thick slab is produced by slow solidification method. The influences on solidification structure and macro segregation under different superheating and cooling intensity have been investigated. Besides, a new method of improving the final quality of ultra-thick slab via slow solidification method is also provided, which has a high development prospect in the production of large-section casting slabs.

2 PARAMETERS OF MODEL

2.1 The Structure of Thick Slab Continuous Caster

In this paper, ultra-thick slabs are produced by thick slab continuous caster. The structure of caster is shown in Fig. 1.

Table 1 The casting parameters of slab continuous caster

Items	Value
Length of continuous caster	44,50 m
Superheating	30 K
Length of mold	0,9 m
Water flow of mold	285 m^3/h (Wide Suface) 44 m^3/h (Narrow Suface)
Specific heat of water	4200 J kg^{-1} K^{-1}
Temperature difference of mold cooling water	5,0 K
Water flow of secondary cooling zone	170 m^3/h (Outer arc) 120 m^3/h (Inner arc)
Casting speed	0,9 m min^{-1}

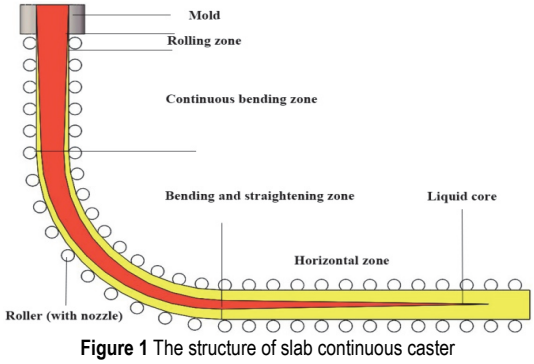

Figure 1 The structure of slab continuous caster

The cooling mechanism of caster is divided into five cooling zones, ie. mold, rolling zone, continuous bending zone, bending and straightening zone and horizontal zone. The nozzles are arranged around the roller, which can provide water cooling on the wide surface of slab. The casting parameters are shown in Tab. 1.

2.2 Materials and Thermal-physical Parameters

Simulations were performed with MJ45, the chemical positions of MJ45 are listed in Tab. 2. The liquidus and solidus temperature are calculated by the material database of ProCAST. The results of liquidus and solidus are 1762 K and 1694 K, respectively.

Table 2 Elements composition of MJ45

Element	C	Mn	P	S	Si
Content / %	0,47	0,75	0,018	0,006	0,25

2.3 Assumptions and Mesh Generation

The governing equation of heat transfer can be concluded as Eq. (1).

$$\rho C\frac{\partial T}{\partial t}=\frac{\partial}{\partial x}\left(\theta\frac{\partial T}{\partial x}\right)+\frac{\partial}{\partial y}\left(\theta\frac{\partial T}{\partial y}\right)+\frac{\partial}{\partial z}\left(\theta\frac{\partial T}{\partial z}\right)+Q \qquad (1)$$

The left part of Eq. (1) is heat change, which is caused by temperature or mass flow. Where ρ is destiny, kg·m^{-3}; C is specific heat, J·kg^{-1}·K^{-1}; T is temperature, K; t is time, s; Q is latent heat J; θ is effective heat transfer coefficient; x, y and z are point coordinates of their axis.

The slice moving boundary model is used in this paper. The length, width and thickness of model are 2200 mm, 300 mm and 20 mm, respectively. By using 10 milimeter hexahedral mesh, 32 836 surface elements and 84 694 volume elements have been generated. The settings of boundary conditions are also shown in Fig. 2. On wide surface, the boundary conditions of mold, secondary cooling and air cooling should be applied as usual. On narrow surface, the mold and air cooling boundary conditions should be provided.

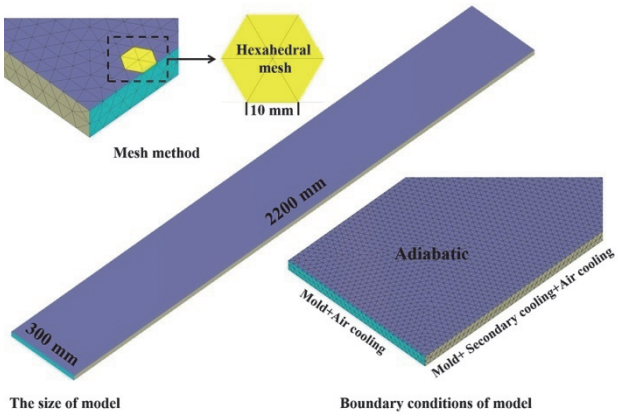

Figure 2 Mesh results and boundary conditions of model

To simplify the process of calculation and simulation, the following assumptions have been provided:
(1) The taper of mold is ignored.
(2) The air gap in mold is ignored.
(3) Artificial water distribution is used in secondary cooling.
(4) The effect of cooling water on the narrow surface is ignored.
(5) Heat transfer along the Z axis is ignored.

2.4 Thermal Boundary Conditions

At the beginning of simulation, the filling percentage of model should be 100 %. Thus, the initial temperature is equal to inlet temperature.

The heat flux of mold can be calculated by Eq. (2).

$$q=\frac{Q_W C_W \Delta T_W}{S_B} \qquad (2)$$

where, Q_w is total water flow of mold cooling water, $L\cdot\text{min}^{-1}$; C_w is the specific heat of water, J·kg^{-1}·K^{-1}; ΔT_w is the temperature difference between the inlet and outlet of mold cooling water, K; S_B is the contacting area between slab and copper staves, m^2.

The film coefficient of secondary cooling zone is related to the specific water flow, which can be concluded as Eq. (3):

$$h_{sec}=aW^b+c_1 \qquad (3)$$

where, W is specific water flow of secondary cooling, L·m^{-2}·s^{-1}; a, b and c_1 are determined by the experiment results. In this paper, a, b, c_1 are 350, 0,351 and 0 respectively.

The heat flux of air cooling zone can be expressed as Eq. (4):

$$q_{rad}=\varepsilon\sigma\left[T_b^4-T_{out}^4\right] \qquad (4)$$

where, ε is blackness, the value is 0,8; σ is the constant of Steven -Boltmann, the value is 5.67 × 10^{-8} W·m^{-2}·K^{-4}; T_b (K) and T_{out} (K) are surface temperature of slab and ambient temperature, respectively,

2.5 Dendrite Growth Model

The "Continuous nucleation model" [11] is improved by Rappaz and Gandin in 1989. The model believed that the nucleation will occur different position in slab. The equation of model is shown in Eq. (5).

$$\frac{\mathrm{d}N}{\mathrm{d}(\Delta T)}=\frac{N_{\max}}{\sqrt{2\pi}\Delta T_\sigma}\cdot exp\left[-\frac{1}{2}\left(\frac{\Delta T-\Delta T_m}{\Delta T_\sigma}\right)^2\right] \qquad (5)$$

where, N and $N_{\max}$ are total and maximum number of grains. ΔT_m (K) and ΔT_σ (K) and average nucleation undercooling and standard deviation of distribution, respectively. ΔT is totally undercooling of the dendrite tips.

During the solidification process, totally undercooling of the dendrite tip is the sum of the constitutional undercooling (ΔT_c), thermodynamics undercooling (ΔT_e), curvature undercooling of solid-liquid interface (ΔT_s) and

growth kinetics undercooling (ΔT_g). The equation can be expressed as follows:

$$\Delta T = \Delta T_c + \Delta T_e + \Delta T_s + \Delta T_g \tag{6}$$

For most of alloys, the total undercooling can be simplified as the function of constitutional undercooling. The speed of dendrite growth can be concluded by Kurz-Giovanola-Trivedi (KGT) model [12], see Eq. (7).

$$V(\Delta T) = a_2 (\Delta T_c)^2 + a_3 (\Delta T_c)^3 \tag{7}$$

where a_2, a_3 are the coefficients of the polynomial of dendrite tip growth velocity, and they can be calculated by ProCAST material database, too. In this paper, a_2 is $9{,}38 \times 10^{-7}$, a_3 is $7{,}95 \times 10^{-7}$.

The SDAS can be calculated by finite element analysis software ProCAST. The SDAS which total content of C is smaller than 0,53 is concluded by B.G.Thomas, see Eq. (8) [13].

$$\lambda_2 = 148(C_R)^{-0.38} \tag{8}$$

where, λ_2 is SDAS, μm; C_R is cooling rate, $K \cdot s^{-1}$

2.6 Macrosegregation Model

Eq. (9), which builds relationship between SDAS and the content of element, has been investigated by Clyne-Kurz [14].

$$C_L = C_0 \left[1 - (1 - 2\alpha k) f_s\right]^{\frac{k-1}{1-2\alpha k}} \tag{9}$$

C_0 and C_L are the initial content of element and the calculated content of element in molten steel, respectively; f_s is fraction solid, %; k is the equilibrium distribution coefficient of solid-liquid phase. A can be calculated by Eq. (10):

$$\alpha = \frac{4D_s}{\lambda_2^2} \cdot \frac{T_L - T_S}{C_R} \tag{10}$$

where D_s is diffusion coefficient in solid; T_L (K) and T_S (K) are liquidus and solidus, respectively.

3 ANALYSIS AND DISCUSSION

3.1 The Validation of Model

The solidification coefficient and the length of liquid core can be calculated by Eq. (11) and Eq. (12)

$$D = Z\sqrt{t_r} \tag{11}$$

$$l = \frac{D^2 v}{Z^2} \tag{12}$$

where, Z is solidification coefficient, $mm \cdot min^{-0.5}$; D is the thickness of solidified shell, mm; v is casting speed, $m \cdot min^{-1}$; t_r (s) and l (m) are running time and running length of slab, respectively.

The nail-shooting experiments were carried out, and the experiment data of solidified shell thickness were exported. The solidification coefficient is obtained by using Eq. (11). Then, substitute the solidification coefficient from Eq. (11) to Eq. (12). The running length of slab is obtained, which can be regarded as the length of liquid core. By the experiment results in production practices, the length of liquid core is 29,62 m. Thermal simulation has been taken, the relationship between running length of slab and fraction solid is shown in Fig. 3. Results show that the maximum running length of slab is 29,88 m, the relative error of simulation value is 0,88%.

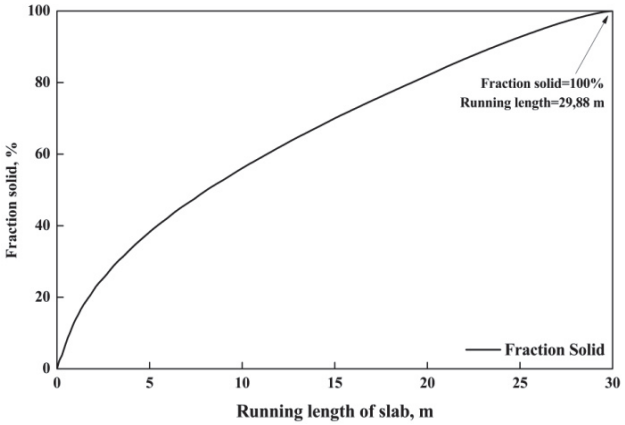

Figure 3 The variation curve of fraction solid during slab solidification

Besides, the macroscopic examination was carried out, too. The experiment result of equiaxed crystal rate is 23,16% [4]. According to the nucleation parameters in Tab. 3, the simulation of solidification structure was also carried out. The simulation result is shown in Fig. 4. Due to the different amount of spray water in wide and narrow surface, the length of columnar crystal on each surface is different, too. According to the simulation, the equiaxed crystal rate of the slab is 23,34%, the relative error of simulation value is 0,77%. By the results above, the simulation results have a high fitting degree of experiment results, and the model can be used for subsequent discussions.

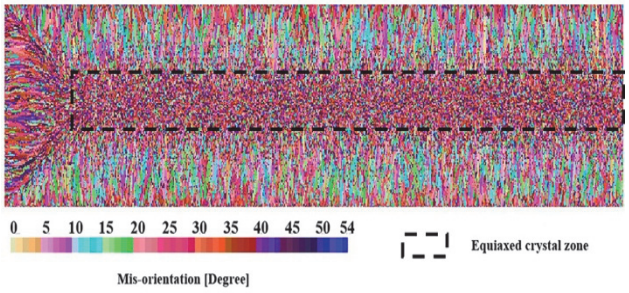

Figure 4 The macro structure of ultra-thick slab

Table 3 Nucleation parameters of model

Nucleation parameters	ΔT_m / K	ΔT_σ / K	N_{max}
Volume	1	0,5	2.5×10^8
Surface	0,5	0,1	1×10^9

3.2 Effect of Superheating and Cooling Intensity on Solidification Structure

3.2.1 Effect of Superheating

In this part, the simulations of solidification structures of ultra-thick slab under different superheating were carried out. The results are shown in Fig. 5.

According to Fig. 5, the solidification structure is divided into three types: chilling layer, columnar crystal and equiaxed crystal. At the beginning of solidification, the heat flux of mold is large, and high undercooling is applied to the solidification front. Though the maximum number of grains is large, there is no space for the nucleation particles to grow. Therefore, the chilling layer is formed. As the undercooling decreases, the dendrites will grow in directed direction. The columnar crystal is generated. At the final stage of solidification, the undercooling is small, and the direction of dendrite growth is uncertain. The nucleation particles begin to generate in all direction. Thus, the equiaxed crystal will be generated. The SDAS has connection with grain size parameters. In following parts, the average grain size, number of grains and equiaxed crystal ratio are exported, see Tab. 4.

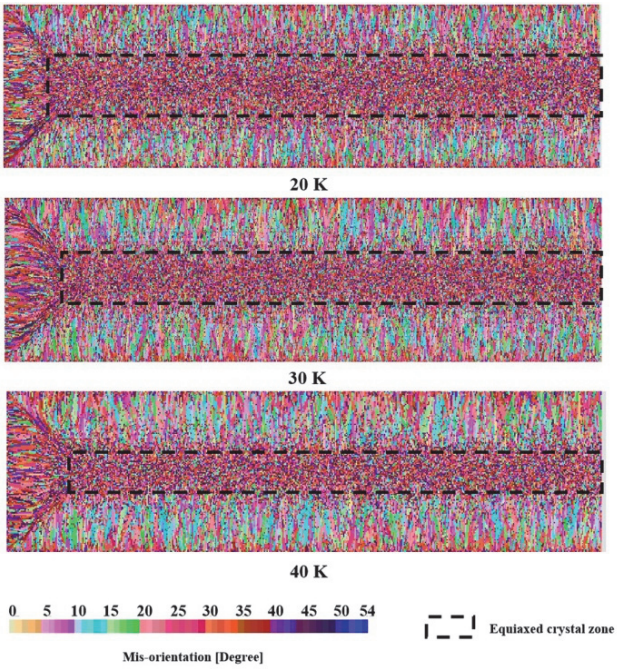

Figure 5 The solidification structure under different superheating

Table 4 The grain properties under different superheating

Superheating / K	Average grain size / μm	Equiaxed crystal ratio	The number of grain
20	1487	37,41%	99 322
30	1530	23,34%	93 219
40	1540	20.62%	85 779

According to Tab. 4, when the superheating increases from 20 K to 40 K, the equiaxed crystal ratio is decreased from 37,41% to 20,62%, and the number of grains is decreased from 99 322 to 85 779. However, the average grain size increases from 1487 μm to 1540 μm, which indicates that a low superheating is beneficial to grain fining.

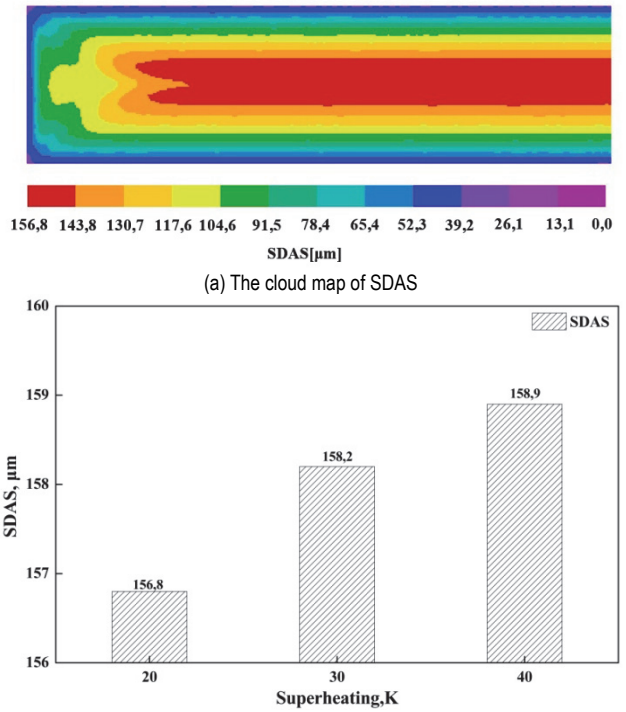

Figure 6 The distribution and result of SDAS

Meanwhile, due to the volume of slab is constant; the DAS will be influenced by the number of grain and the average grain size. The statistic results of SDAS are shown in Fig. 6. It can be seen from the cloud map of SDAS that the value of SDAS is increased from surface to center. When the superheating increases from 20 K to 40 K, the SDAS is increased from 156,8 μm to 158,9 μm. In conclusion, The SDAS is increased with decreasing number of grain and increasing average grain size.

3.2.2 Effect of Cooling Intensity

In this part, the total water flow of secondary cooling has been risen. Besides, the grain properties were shown in Tab. 5. The solidification structures under different cooling intensity were shown in Fig. 7.

It can be concluded from Fig. 7 and Tab. 5 that the equiaxed crystal ratio decreases with increasing cooling intensity. When the cooling intensity increases from weak to strong, the equiaxed crystal ratio decreases from 23,34% to 13,93%. The SDAS and average grain size increases with increasing cooling intensity. The results reported the similar effect of changing superheating.

Table 5 The grain properties under different cooling intensity

Total water flow of secondary cooling zone	170 m^3/h (Outer arc) 120 m^3/h (Inner arc)	272 m^3/h (Outer arc) 192 m^3/h (Inner arc)	340 m^3/h (Outer arc) 240 m^3/h (Inner arc)
Coolant level	Original	Mid-strong	Strong
Average grain size	1530	1543	1552
Equiaxed crystal ratio	23,34%	15,77%	13,93%
Number of grains	93 219	91 895	90 138
SDAS	158,2	178,5	203,3

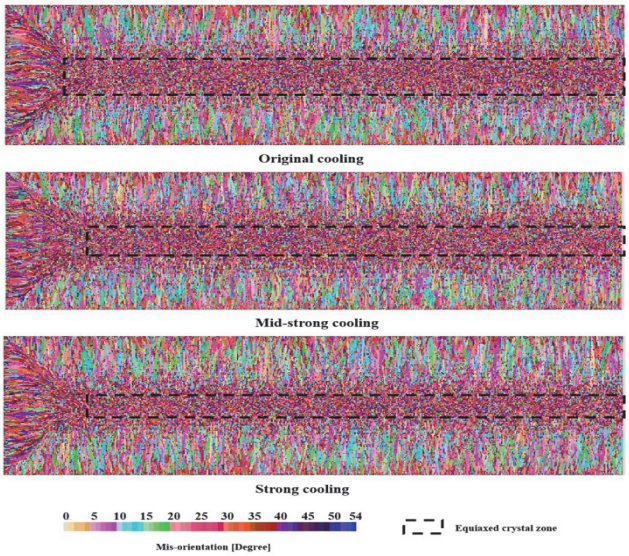

Figure 7 The solidification structure in different cooling intensity

According to the discussions in 3,2; the effect of superheating and cooling intensity on equiaxed crystal ratio and SDAS is linear. Lower superheating and cooling intensity are conducive to grain refinement and reducing the SDAS. The internal quality of the slab can be improved. In the following discussions, the influence on macrosegregation has been concerned.

3.3 Effect of Superheating and Cooling Intensity on Macro Segregation

The effect on element distribution has been also researched. The distribution of carbon (C) is investigated, and the cloud maps of content of carbon under different superheating are shown in Fig. 8. The nodes have been taken along the center-line of wide surface every 100 mm, and the content of C is noted. The distribution of C is shown in Fig. 9.

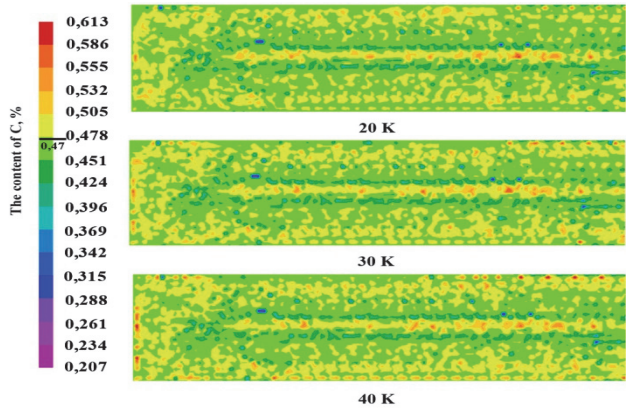

Figure 8 The content of C under different superheating

It can be concluded from Fig. 9 that the high level positive segregation will generate around the center of slab. The reason can be concluded as solute concentration. Due to the high cooling intensity of mold, the cooling rate is fast, and the solute redistribution cannot be carried out in time. The residual solute will be pushed to the solidification front, causing center positive segregation of slab. Results also show that when superheating decreases from 40 K to 20 K, the fluctuation of C is improved.

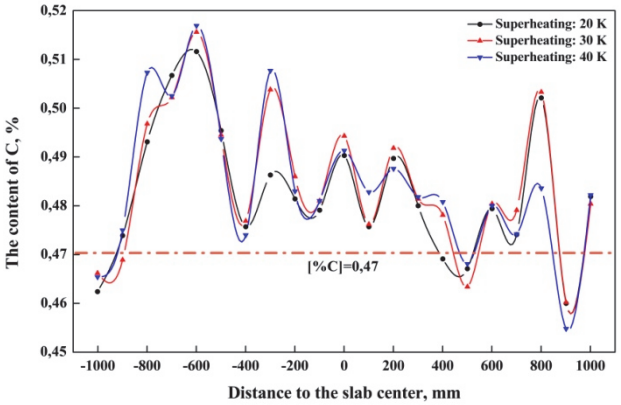

Figure 9 The content of C in center-line direction under different superheating

The content of C in different cooling intensity is shown in Fig. 10. The curves in Fig. 10 showed that the positive segregation can be improved by using mid-strong cooling. The segregation indicators: including maximum, minimum, average content of C; segregation ratio and segregation degree, are listed in Tab. 6.

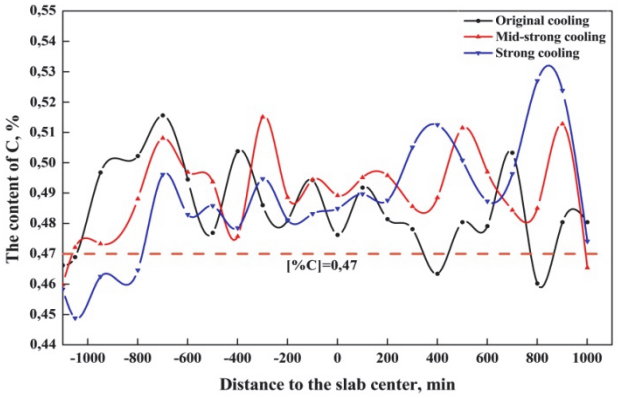

Figure 10 The content of C in center-line direction under different cooling intensity

According to Tab. 6, when the cooling intensity increases from original to strong, the segregation ratio and segregation degree first decreased then increased. When mid-strong cooling is provided, the segregation ratio is 1,3836; and the segregation degree is 0,3196. The lower segregation indicator has been created by mid-strong water flow of secondary cooling zone.

Table 6 The segregation indicator of ultra-thick slab

Coolant level	Original	Mid-strong	Strong
Maximum content of C (C_{max})	0,5720	0,5680	0,5715
Minimum content of C (C_{min})	0,3992	0,4105	0,4069
Average content of C (C_{ave})	0,4890	0,4927	0,4951
Segregation ratio (C_{max}/C_{min})	1,4331	1,3836	1,4045
Segregation degree (C_{max}/C_{ave})	0,3535	0,3196	0,3325

The discussions above show that the effect of superheating on the carbon distribution in the center-line of slab is relatively small. Comparing with the results, the segregation is improved at a superheating of 20 K. The cooling intensity has a greater influence on the center-line segregation. The segregation can be improved by applying mid-strong cooling. Several experiments were carried out in production field, with low superheating and mid-cooling intensity; the defect rating of ultra-thick continuous casting slabs has been improved.

4 CONCLUSION

In this paper, the slice of moving boundary model is used and the solidification structure and macrosegregation are simulated. According to the discussion above, the following conclusions can be concluded:

1) The SDAS is increased with increasing superheating and cooling intensity. When superheating increases from 20 K to 40 K, the SDAS is increased from 156,8 μm to 158,9 μm. The effect of increased SDAS is more obvious by changing cooling intensity; when strong cooling is provided, the SDAS increases from 158,2 μm to 203,3 μm. Lower superheating and cooling intensity are conducive to grain refinement and reducing the SDAS. The internal quality of the slab can be improved.

2) The segregation will be improved by decreasing superheating and mid-strong cooling intensity. When superheating increases from 20 K to 40 K, the center positive segregation will be improved. When mid-strong cooling intensity is provided, the segregation ratio decreases from 1,4331 to 1,3836, and the segregation degree decreases from 0,3535 to 0,3196.

3) Researches in 3,2 and 3,3 show that the use of low superheating can refine the grains, the macro segregation in the center-line of wide surface can be improved by adding mid-strong cooling intensity. The research provides new methods to improve the quality of slow solidification ultra-thick slabs, which has a high development prospect in the production of large-section casting slabs.

Acknowledgement

The authors are grateful for the financial support from the National Natural Science Foundation of China (No. 51504130) and Joint Fund of HGSKL-USTLN (No. HGSKL-USTLN (2020)02), Partial support was also provided by Special Fund of USTL (No. 2017HZ01) and USTL Talent Project (No. 601011507-15).

5 REFERENCES

[1] Han, J., Fu, T. L., Wang, Z. D., & Wang, G. D. (2020). Effect of Roller Quenching on Microstructure and Properties of 300 mm Thickness Ultra-Heavy Steel Plate. *Metals*, *10*, 1238-1250. https://doi.org/10.3390/met10091238

[2] Wang, Z. D., Wang, B. X., Wang, B., Tian, Y., Zhang, T., Yuan, G., Liu, Z. Y., & Wang, G. D. (2019). Development and Application of Thermo-mechenical Control Process Involving Ultra-fast Cooling Technology in China. *ISIJ International*, *59*(12), 2131-2141. https://doi.org/10.2355/isijinternational.ISIJINT-2019-041

[3] Tsuyama, S. (2015). Thick Plate Technology for the Last 100 Years: A World Leader in Thermo Mechanical Control Process. *ISIJ international*, *55*(1), 67-78. https://doi.org/10.2355/isijinternational.55.67

[4] Zhang, L. W., Xu, C. J., Li, J., Yang B., & Li, S. L. (2017). Effect of Slow Solidification Rate on Macrostructure of the Ultra-thick Slab.(Eds.). (2017). *Conference Proceedings of the 7th International Conference on Modelling and Simulation of Metallurgical Processes in Steelmaking*, 244-247.

[5] Yang, B. (2019). Study on Slow Solidification Process and Quality Characteristics of Ultra-thick Slab.(in Chinese) https://kns.cnki.net/KCMS/detail/detail.aspx?dbname=CMFD202001&filename=1019255188.nh.

[6] Xiao, C., Zhang J. M., Luo, Y. Z., Wei, X. D., Wu, L., & Wang S. X. (2013). Control of Macrosegregation Behavior by Applying Final Electromagnetic Stirring for Continuously Cast High Carbon Steel Billet. *Journal of Iron and Steel Research, International.*, *20*(11), 13-20. https://doi.org/10.1016/S1006-706X(13)60190-9

[7] Dong, P. L., Shang, H. X., & Wang, H. (2017). Typical Quality Defect Cause and Control Technology of Slab and Plate. *China Metallurgy*, *27*(6), 7-13.

[8] An, G. Y. & Liu, L. X. (1987). Dendrite spacing in unidirectionally solidified Al-Cu alloy. *Journal of Crystal Growth*, *80*, 383-392. https://doi.org/10.1016/0022-0248(87)90085-6

[9] Osorio, W. R., Spinelli, J. E., Cheung, N., & Garcia, A. (2006). Secondary dendrite arm spacing and solute redistribution effects on corrosion resistance of Al-10 wt% Sn and Al-20 wt% Zn alloys, *Materials Science and Engineering A*, *420*, 179-186. https://doi.org/10.1016/j.msea.2006.01.058

[10] Long, M. J., Zhang, L. F., & Lu, F., (2010). A simple model to calculate dendrite growth rate during steel continuous casting process, *ISIJ International*, *50,* 1792-1796. https://doi.org/10.2355/isijinternational.50.1792

[11] Tan, Y. M. & Wang, H. F. (2012). Modeling Constrained Dendrite Growth in Rapidly Directional Solidification. *Journal of Materials Science*, *47*(13), 5308-5316. https://doi.org/10.1007/s10853-012-6417-z

[12] Kurz, W., Giovanola, B., & Trivedi, R. (1986). Theory of microstructural development during rapid solidification. *Acta Metallurgical*, *34*(5), 823-830. https://doi.org/10.1016/0001-6160(86)90056-8

[13] El-Bealy, M. & Thomas, B. G. (1996). Prediction of dendrite arm spacing for low alloy steel casting processes. Metallurgical and *Materials Transactions B*, *27*(B), 688-693. https://doi.org/10.1007/BF02915668

[14] Clyne, T. W. & Kurz, W. (1981). Solute redistribution during solidification with rapid solid state diffusion. *Metallurgical Transactions A*, *12*(6), 965-971. https://doi.org/10.1007/BF02643477

Contact information:

Jia-zheng ZHANG, Postgraduate
School of Materials and Metallurgy, University of Science and Technology Liaoning, Anshan, People's Republic of China
State Key Laboratory of Metal Material for Marine Equipment and Application E-mail: kapok1a96@163.com

Ling YAN, Senior engineer
State Key Laboratory of Metal Material for Marine Equipment and Application
Anshan, Liaoning Province, People's Republic of China
E-mail: geqeg801ycnc2@163.com

Chang-jun XU, PhD, Assistant Professor
(Corresponding author)
School of Materials and Metallurgy, University of Science and Technology Liaoning, Anshan, People's Republic of China
E-mail: jassonas@163.com

De-jun LI, Senior engineer
(Corresponding author)
State Key Laboratory of Metal Material for Marine Equipment and Application
Anshan, Liaoning Province, People's Republic of China
E-mail: 416177019@qq.com

Lian-wang ZHANG, PhD
School of Materials and Metallurgy, University of Science and Technology Liaoning, Anshan, People's Republic of China
E-mail: zhanglianwang92@163.com